Abdominal Radiology (2022) 47:1817–1827
https://doi.org/10.1007/s00261-022-03471-y

HEPATOBILIARY

Assessment of dynamic hepatic and renal imaging changes in COVID-19 survivors using T1 mapping and IVIM-DWI

Qiuyue Han[1,2] · Yiping Lu[2] · Dongdong Wang[2] · Yajing Zhao[2] · Xuanxuan Li[2] · Nan Mei[2] · Yuqi Zhu[2] · Anling Xiao[3] · Bo Yin[2]

Received: 10 December 2021 / Revised: 20 February 2022 / Accepted: 21 February 2022 / Published online: 13 March 2022

Abstract

Purpose To explore the imaging changes of the liver and kidneys in COVID-19 survivors using variable flip angle (VFA) T1 mapping and intravoxel incoherent motion-diffusion weighted imaging (IVIM-DWI).

Methods This prospective study included 37 discharged COVID-19 participants and 24 age-matched non-COVID-19 volunteers who underwent abdominal MRI with VFA T1 mapping and IVIM-DWI sequencing as a COVID-19 group and control group, respectively. Among those discharged COVID-19 participants, 23 patients underwent two follow-up MRI scans, and were enrolled as the 3-month follow-up group and 1-year follow-up group, respectively. The demographics, clinical characteristics, and laboratory tests were collected. Imaging parameters of the liver and kidneys were measured. All collected values were compared among different groups.

Results The 3-month follow-up group had the lowest hepatic T1 value, which was significantly lower than the value in the control group ($P < 0.001$). Additionally, the 3-month follow-up group had the highest hepatic ADC and D values, cortical ADC and f values, which were significantly higher than those in the control group (for all, $P < 0.05$). The hepatic D value in the 1-year follow-up group decreased significantly in comparison with that in the 3-month follow-up group ($P = 0.001$). Compared to non-severe patients, severe cases had significantly higher hepatic D* and f*D* values ($P = 0.031$, $P = 0.015$, respectively).

Conclusion The dynamic alterations of hepatic and renal imaging parameters detected with T1 mapping and IVIM-DWI suggested that COVID-19 survivors might develop mild, non-symptomatic liver and kidney impairments, of which liver impairment could probably relieve over time and kidney impairment might be long-existing.

Qiuyue Han and Yiping Lu contributed equally to this work.

✉ Anling Xiao
xiaoanlingmd@163.com

✉ Bo Yin
yinbo@fudan.edu.cn

[1] Shanghai Institute of Medical Imaging, 180 Feng Lin Rd, Shanghai 200032, China

[2] Department of Radiology, Huashan Hospital, Fudan University, 12, Middle Wulumuqi RdJing'an District, Shanghai 200040, China

[3] Department of Radiology, FuYang No. 2 People's Hospital, 450 Linquan Road, Fuyang 236415, Anhui, China

Graphical abstract

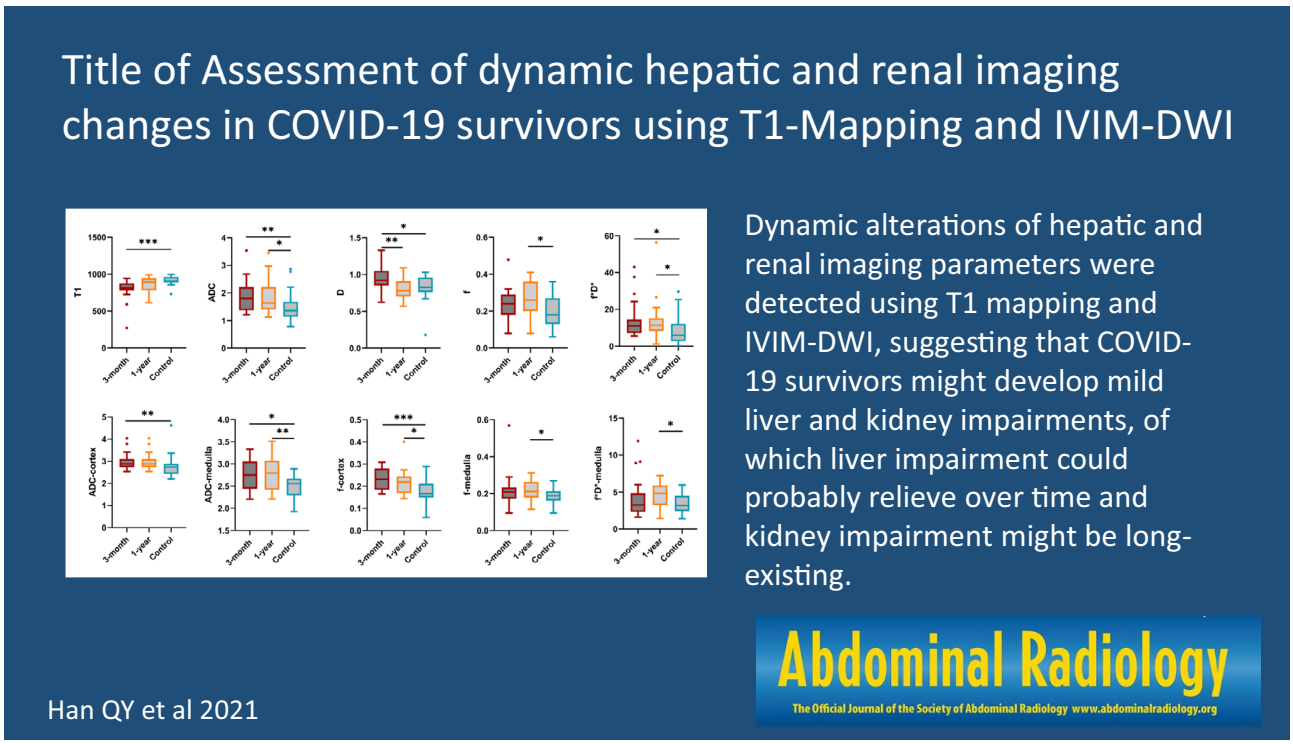

Keywords COVID-19 · Dynamic alterations · T1 mapping · IVIM-DWI

Introduction

Coronavirus disease 2019 (COVID-19) is caused by a novel coronavirus called severe acute respiratory syndrome coronavirus 2 (SARS-CoV-2), which has created a global health crisis [1]. Although the lungs are the major organs attacked by SARS-CoV-2, other organs such as the liver and kidneys can also be damaged in patients with COVID-19 [2–4]. For example, abnormal liver and kidney function tests have been found in many COVID-19 patients without pre-existing liver and kidney disease on admission [2, 5]. In addition, inflammatory changes and vesicular steatosis of liver parenchyma as well as proximal acute tubule injury and endothelial cell swelling of the kidneys have been reported in pathological examinations of COVID-19 patients [4].

Noninvasive functional MRI can provide both morphologic and functional liver and kidney assessment during the development of acute injury [6], thereby assisting in the detection and evaluation of early damage. As T1 mapping is a sequence sensitive to signal changes, and intravoxel incoherent motion-diffusion weighted imaging (IVIM-DWI) can detect diffusion and perfusion at the same time, we chose these two techniques to explore liver and kidney changes in COVID-19 survivors.

T1 mapping is a quantitative technique which can directly measure the T1 relaxation time in milliseconds [7], depicting even small variations of T1 relaxation time within a tissue [8]. The early changes in acute tissue injury such as interstitial edema usually lengthen the T1 relaxation time, whereas fat deposition and iron overload shorten the T1 time. Recently published studies have reported that T1 mapping could be used for the assessment of liver diseases such as liver fibrosis and non-alcoholic fatty liver disease [8, 9]. IVIM-DWI separates pure molecular diffusion (D) from perfusion-dependent diffusion [10], which is measured by the perfusion-related pseudo-diffusion coefficient (D*) and the perfusion fraction (f). As a non-invasive technique, IVIM-DWI has great potential for diagnosing hepatic lesions and evaluating treatment responses in liver cirrhosis [11]. In addition, IVIM-DWI can detect differences between the renal cortex and medulla [12, 13], which indicates its utility in detecting renal perfusion changes.

Recently, several attempts have been made to evaluate liver and kidney injuries in COVID-19 patients using CT or dual-energy CT [14, 15]. As far as we know, there has been no study on the assessment of liver or kidney MRI changes in COVID-19 patients. One reason may be that MRI examinations have been limited during the outbreak period

of COVID-19 to prevent the spread of the disease. Thus, we carried out this short-term and long-term follow-up study to explore the existence and dynamic changes of hepatic and renal injuries in COVID-19 survivors using T1 mapping and IVIM-DWI.

Materials and methods

Study design and patient population

This was a prospective study approved by our local ethics institutional review board. Informed consent was obtained from all the participants before performing MRI scans.

A total of 40 discharged COVID-19 participants hospitalized between January 21 and March 3, 2020 were recruited and underwent abdominal MRI scans three months after discharge, including VFA T1 mapping and IVIM-DWI. Three patients were excluded. The remaining 37 participants (average age: 53.7 ± 12.5 years; male: 54.1%) were included in this study as the COVID-19 group. Although all enrolled participants were required to undergo second-time follow-up scans, only 23 patients (average age: 50.9 ± 10.8 years; male: 56.5%) from the COVID-19 group underwent another abdominal MRI nine months later (the rest were unable to attend the follow-up due to personal reasons). 23 patients who underwent follow-up MRI scans at 3-month and 1-year after discharge were enrolled as the 3-month follow-up group and 1-year follow-up group, respectively. Additionally, 24 age-matched (± 5 years) volunteers (average age: 57.1 ± 15.0 years; male: 41.7%) without pre-existing hepatic and renal diseases were enrolled as the control group. The volunteers were recruited through social media and all agreed to undergo MRI scans. Before scanning, a questionnaire on basic clinical information mainly concerning liver and kidney condition was completed by each participant, including the history of drinking. The baseline demographics, clinical characteristics during hospitalization and laboratory tests at admission and 3-month follow-up of all participants and laboratory studies of the 23 participants at 1-year follow-up were collected. The diagnosis and discharge criteria of COVID-19 patients were made according to the Guidelines for Diagnosis and Treatment of COVID-19 issued by the National Health Commission (7th edition) (in Chinese) [16]. The COVID-19 group ($n = 37$) and the 1-year follow-up group ($n = 23$) was further divided into the severe and the non-severe cases based on the guidelines. The protocol of the study is presented in Fig. 1.

MRI acquisition

All examinations were performed on a clinical 3.0 T MRI system (Skyra, Siemens Medical Solutions, Erlangen, Germany) with an 18-channel phased-array body coil. Axial VFA T1 mapping and IVIM-DWI were performed.

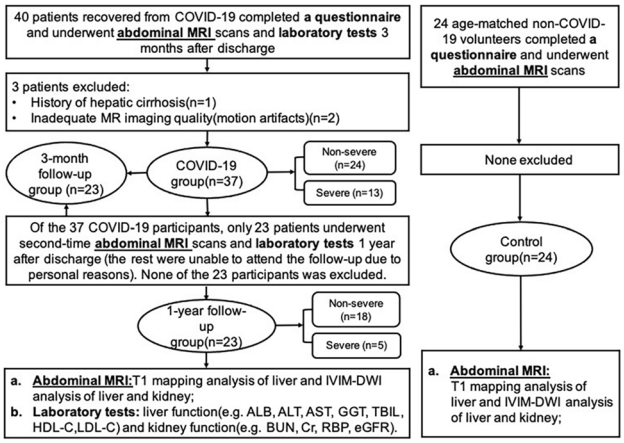

Fig. 1 Protocol of the study

T1 mapping

For T1 mapping, a dual flip angle 3D gradient echo sequence with volumetric interpolated breath-hold examination (VIBE) was performed without injection of contrast agent. The parameters were as follows: repetition time, 5.01 ms; echo time, 2.3 ms; flip angle, 5° and 10°; field of view, 380 × 380 mm; acquisition matrix, 135 × 224 mm; bandwidth, 300 Hz; slice thickness, 4 mm.

IVIM-DWI

IVIM was performed using a free-breathing single-shot, spin-echo, echo-planar imaging sequence in three orthogonal directions with the following parameters: TR/TE, 4400/60 ms; slice thickness, 4 mm; spacing between slices, 4.8 mm; field of view, 400 × 400 mm; acquisition matrix, 100 × 134 mm; bandwidth, 2332 Hz; and images were acquired with 12 b-values (0, 10, 20,30, 40, 50, 80, 100, 200, 400, 800, and 1000 s/mm^2). The distribution of b-values was chosen to cover both the initial pseudo-diffusion decay ($b < 200$ s/mm^2) and the molecular diffusion decay ($b > 200$ s/mm^2).

Image analysis

T1 mapping

The T1 mapping MR data series was transferred to the workstation to measure the T1 relaxation time of the liver parenchyma on a pixel-by-pixel basis on a color distribution map by using Functool software (AW 4.6, GE Healthcare). Round regions of interest (ROIs) with a range of 200 mm^2

were drawn manually in the liver on T1 mapping images. Five ROIs were placed in the right lobe of the liver away from the liver edge, devoid of obvious vessels, bile ducts, focal lesions, and imaging artifacts (Fig. 2a). The left lobe was not included because of the potential dephasing artifacts from cardiac motion [17]. The mean T1 relaxation time of the five ROIs was considered as the representative T1 relaxation time for the liver.

IVIM-DWI

All IVIM-DWI data were transferred to an independent personal computer and processed offline with a dedicated software package (FireVoxel; CAI2R; New York University, NY) for quantitative analyses. Five round hepatic ROIs with a range of 200 mm^2 were sparsely drawn in different slices and lobes of liver parenchyma on IVIM-DWI, devoid of obvious vessels, bile ducts, focal lesions, and imaging artifacts (Fig. 2b). Renal ROIs were manually drawn bilaterally on perihilar slices in the cortex and medulla of both kidneys. Cortical ROIs followed the outer contour of the kidney, avoiding artifacts and lesions (Fig. 2c). Medullary ROIs were drawn in the inner region of the renal parenchyma, avoiding artifacts, major vessels, lesions, and renal fat (Fig. 2d).

Signals were averaged for all voxels inside an ROI of the same type, and were then fitted by a Bayesian algorithm to the IVIM Eq. (1) to obtain the diffusion coefficient D ($\times 10^{-3}$ mm^2/s), the pseudo-diffusion coefficient D* ($\times 10^{-3}$ mm^2/s), the perfusion fraction f and f*D* ($\times 10^{-3}$ mm^2/s). The standard ADC ($\times 10^{-3}$ mm^2/s) was obtained by using the conventional mono-exponential model with all b-values (Eq. 2). Quantitative parameters (D, D*, f, f*D*) derived from IVIM MRI were automatically obtained.

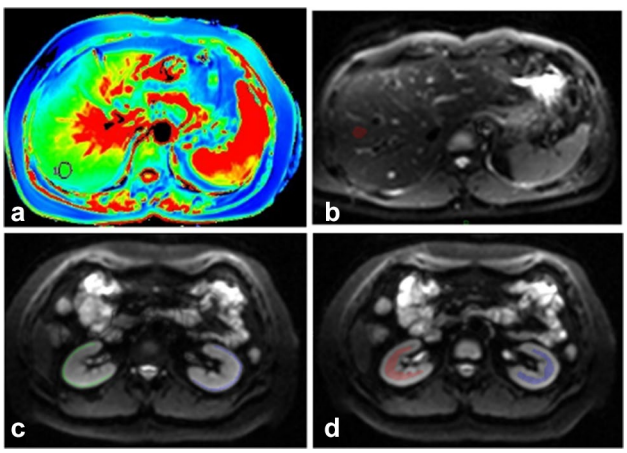

Fig. 2 Schematic diagram of ROI drawing. **a** One ROI of liver drawn on T1 mapping. **b-d** IVIM-DWI. One ROI of liver outlined on b = 0 (**b**) and ROIs of renal cortex (**c**) and medulla (**d**) outlined on b = 50

$$S = S0 * (f * \exp(-b * D^*) + (1 - f) * (\exp(-b * D)) \quad (1)$$

$$S = S0 * \exp(-b * ADC) \quad (2)$$

Two different radiologists independently completed the ROI delineation of the COVID-19 group according to the above principles. The intraclass correlation coefficient (ICC) values between two groups were used to quantify the consistency (The details were in the supplementary materials).

Statistical analysis

All statistical analyses were carried out with IBM SPSS Statistics (v. 26.0, Chicago, IL). Data normality was assessed by the Shapiro–Wilk test. The differences of continuous variables with a skewed distribution were compared using the Mann–Whitney U-test for independent variables or Wilcoxon Signed Rank Test for paired variables. Chi-square test were used to compare categorical variables. The differences of continuous variables with a normal distribution were evaluated using the independent sample t test. A two-way ANOVA analysis followed by a Bonferroni multiple comparison test was used for laboratory tests obtained at different periods. Box plots were carried out using GraphPad Prism (version 9.2.0.332). The normal-distribution data were expressed as mean ± standard deviation or mean (95% CI). The skewed-distribution data were expressed as median and interquartile range. Categorical variables were expressed as numbers and percentages. The *P* value was two-sided, and a difference of $P < 0.05$ was considered statistically significant.

Results

Baseline demographics and clinical characteristics of all participants

A total of 40 participants who had recovered from COVID-19 were recruited and underwent follow-up abdominal MRI three months after discharge. One participant with a history of hepatic cirrhosis ($n = 1$) and two participants with inadequate MR imaging quality (motion artifacts) ($n = 2$) were excluded. The mean durations from discharge to abdominal MRI examination of the COVID-19 group and 1-year follow-up group were 93.2 ± 12.7 days and 362.6 ± 23.2 days, respectively. No differences in age, gender, or drinking history were detected between the 1-year follow-up group and control group ($P = 0.142$, 0.387, 1.000, respectively) (Table 1).

Table 1 Clinical characteristics of COVID-19 group, 1-year follow-up group, and control group participants

Parameters	COVID-19 ($n=37$)	1-year follow-up ($n=23$)	Control ($n=24$)	P
Age(years)	53.7 ± 12.5	50.9 ± 10.8	57.1 ± 15.0	0.142
Patient data (%)				
No. of men	20 (54.1)	13 (56.5)	10 (41.7)	0.387
No. of women	17 (45.9)	10 (43.5)	14 (58.3)	
Drinking history	5	3	3	1.000
Course severity (%)				
Non-severe	24 (64.9)	18 (78.3)	NA	NA
Severe	13 (35.1)	5 (21.7)	NA	
Duration from discharge to abdominal MRI (days)	93.2 ± 12.7	362.6 ± 23.2	NA	NA
Comorbidities (%)				
Chronic liver disease	0	0	0	NA
Chronic renal disease	0	0	0	NA
Hypertension	7 (18.9)	3 (13.0)	4 (16.7)	1.000
Diabetes	5 (13.5)	1 (4.3)	3 (12.5)	0.609
Coronary artery disease	1 (2.7)	0	0	NA
Cerebrovascular disease	1 (2.7)	0	0	NA
Chronic obstructive pulmonary disease	1 (2.7)	0	0	NA
Treatment before discharge				
Antiviral therapy	37 (100)	23 (100)	NA	NA
Glucocorticoid therapy	3 (8.1)	1 (4.3)	NA	NA

Data are expressed as mean ± standard deviation for continuous variables, and number and percentage (in parentheses) for categorical variables

P values were comparisons between 1-year follow-up group and control group calculated with independent sample t test for continuous variables or Chi-square test for categorical variables

*$P<0.05$ is considered to be statistically different

NA not applicable

Biochemical indexes of COVID-19 participants

The laboratory tests of the 23 COVID-19 participants with two follow-ups performed at admission, at 3-month follow-up, and at 1-year follow-up are shown in Table 2. ALB, AST, GGT, HDL-C, LDL-C, BUN, and Retinol-Binding Protein (RBP) were within normal range or showed mild abnormalities at admission, and significant differences among these three periods were detected (for all, $P<0.05$). No differences in ALT, TBIL, Creatinine, or estimated glomerular filtration rate (eGFR) were found (for all, $P>0.05$). The laboratory testing results were also compared between the non-severe and severe cases in the COVID-19 group (Table 3). Blood urea nitrogen (BUN) showed a significant difference between the severe cases and non-severe cases ($P=0.008$), although it was within a normal range in each group. The rest of the indexes showed no differences (for all, $P>0.05$).

T1 mapping and IVIM-DWI findings of liver

An escalating trend of T1 relaxation time and a declining trend of ADC were observed in the sequence of the 3-month follow-up group to the 1-year follow-up group to the control group. The D value of the 3-month follow-up group was higher than that of the 1-year follow-up group and the control group ($P=0.001$ and 0.010, respectively). The f value in 1-year follow-up group was elevated compared to the control group ($P=0.019$). The hepatic D* value showed no differences among the three groups ($P>0.05$). Detailed comparisons among the three groups were illustrated in Fig. 3. The typical cases from different groups were shown in Fig. 4 and Fig. 5.

Table 4 presents a comparison of hepatic T1 and IVIM parameters between the non-severe and severe cases in the COVID-19 group. Severe cases had higher D* and f*D* values than non-severe cases ($P=0.031$ and 0.015, respectively). The typical non-severe and severe cases were shown in Fig. 6. No differences of T1, ADC, D, or f values were found (for all, $P>0.05$). Hepatic T1 and IVIM parameters between the non-severe and severe cases in the 1-year follow-up were also compared, but no significant difference was detected (Table S3).

Table 2 Comparisons of laboratory parameters of the 23 COVID-19 participants with two follow-ups at admission, at 3-month follow-up and at 1-year follow-up

Laboratory tests	At admission ($n=23$)	3-month ($n=23$)	1-year ($n=23$)	P
Albumin (ALB) (g/L)	40.7 (39.8,41.6)	45.7 (44.7,46.6)	45.9 (44.9,46.9)	< 0.001*
ALT (U/L)	30.0 (23.2,36.7)	27.7 (17.1,38.2)	24.1 (17.7,30.5)	0.236
AST (U/L)	30.1 (25.9,34.3)	22.1 (19.4,24.9)	20.6 (18.8,22.5)	< 0.001*
GGT (U/L)	44.6 (30.1,59.1)	30.7 (19.2,42.2)	27.3 (14.8,39.9)	0.032*
TBIL (μmol/L)	12.4 (9.7,15.0)	12.2 (10.0,14.3)	14.1 (10.0,18.1)	0.281
HDL-C (mmol/L)	1.1 (1.0,1.2)	1.2 (1.1,1.3)	1.3 (1.2,1.4)	0.003*
LDL-C (mmol/L)	2.3 (2.0,2.5)	2.6 (2.4,2.8)	2.9 (2.6,3.1)	< 0.001*
BUN (mmol/L)	4.1 (3.6,4.6)	5.4 (4.8,6.0)	5.2 (4.6,5.8)	< 0.001*
Creatinine (Cr) (μmol/L)	66.8 (60.7,72.9)	63.3 (58.2,68.5)	62.0 (54.6,69.5)	0.421
Retinol-Binding Protein (RBP) (mg/L)	24.8 (21.6,28.1)	32.3 (28.6,36.0)	34.9 (30.7,39.1)	< 0.001*
eGFR (ml/min)	119.6 (108.0,131.1)	123.5 (114.6,132.5)	129.1 (115.4,142.7)	0.425

Data are expressed as mean and 95%CI (in parentheses) for continuous variables

P values among laboratory tests obtained at different periods (at admission, at 3-month follow-up and at 1-year follow-up) were calculated with two-way ANOVA analysis followed by a Bonferroni multiple comparison test

*$P < 0.05$ is considered to be statistically different. Normal range: Albumin (ALB), 40–55 g/L; ALT = Alanine aminotransferase, 7–40 U/L; AST = Aspartate aminotransferase, 15–35 U/L; GGT = γ-glutamyl transpeptidase, 7–45 U/L; TBIL = Total bilirubin, 0–21 μmol/L; HDL-C = High-density lipoprotein cholesterol, 1.04–1.68 mmol/L; LDL-C = Low-density lipoprotein cholesterol, 0–3.36 mmol/L; BUN = Blood urea nitrogen, 2.6–7.5 mmol/L; Creatinine (Cr), 35–115 μmol/L; Retinol-Binding Protein (RBP), 25–70 mg/L; eGFR = Estimated glomerular filtration rate, 80–120 ml/min

Table 3 Baseline clinical and laboratory parameters at 3-month follow-up are shown of non-severe and severe participants in the COVID-19 group

Parameters	Non-severe ($n=24$)	Severe ($n=13$)	P
Age(years)	51.7 ± 12.3	58.5 ± 12.2	0.138
Patient data (%)			
No. of men	13 (52.0)	8 (66.6)	0.491
No. of women	12 (48.0)	4 (33.3)	
Albumin (ALB)(g/L)	45.6 (44.7,46.5)	45.3 (43.6,46.9)	0.674
ALT (U/L)	29.3 (19.4,39.2)	26.6 (13.1,40.1)	0.886
AST (U/L)	22.9 (20.3,25.5)	24.5 (14.7,34.3)	0.327
GGT (U/L)	32.1 (21.5,42.7)	27.8 (19.3,36.2)	0.835
TBIL (μmol/L)	11.6 (9.6,13.6)	10.2 (7.4,13.0)	0.412
HDL-C (mmol/L)	1.2 (1.1,1.3)	1.1 (0.9,1.3)	0.583
LDL-C (mmol/L)	2.7 (2.5,2.9)	2.6 (2.4,2.9)	0.843
BUN (mmol/L)	5.1 (4.6,5.6)	6.5 (5,4,7.5)	0.008*
Creatinine (Cr) (μmol/L)	62.0 (57.4,66.5)	64.6 (57.3,71.9)	0.509
Retinol-Binding Protein (RBP) (mg/L)	32.0 (28.3,35.6)	38.5 (32.0,45.0)	0.051
eGFR (ml/min)	125.4 (117.4,133.4)	121.2 (107.5,134.8)	0.553

Data are expressed as mean and 95%CI (in parentheses) for continuous variables and percentage (in parentheses) for categorical variables

P values between non-severe and severe cases were calculated with Mann–Whitney U-test

*$P < 0.05$ is considered to be statistically different

IVIM-DWI Findings of Kidneys

In all participants, the left and right renal parenchyma exhibited similar IVIM-DWI parameters (for all, $P > 0.05$). Thus, the parameters of bilateral kidneys were averaged and used for further analysis. In all three groups, the D values from the cortex were higher than those from the medulla (for all, $P < 0.01$) (Table S1).

Cortical ADC and renal f values in the 3-month follow-up group were the highest among the three groups

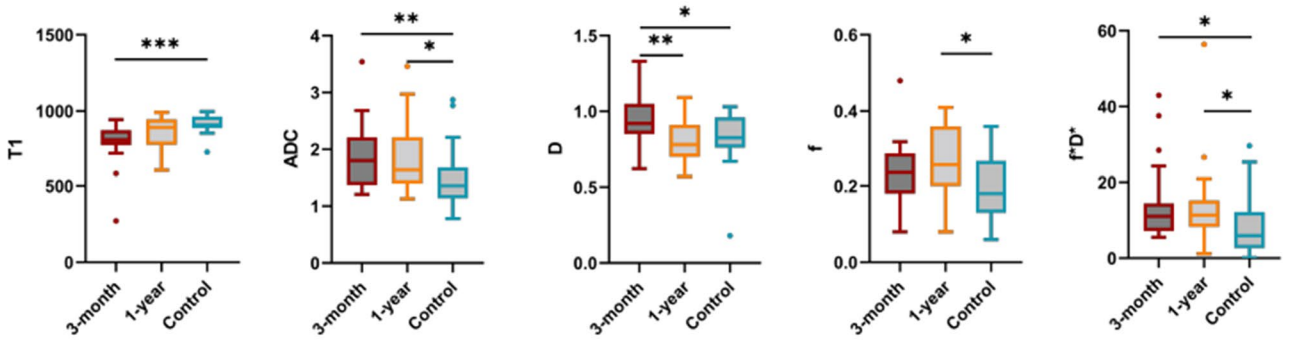

Fig. 3 Boxplots of T1 mapping and IVIM-MRI parameters in the liver of the three groups (*$P<0.05$; **$P<0.01$, ***$P<0.001$). Parameters without significant difference are not listed. *P* values between two independent groups were calculated using Mann–Whitney U-test. *P* values between paired variables (3-month follow-up group and 1-year follow-up group) were calculated using Wilcoxon Signed Rank Test. 3-month: 3-month follow-up group; 1-year: 1-year follow-up group; Control: control group. T1: msec; ADC: $\times 10^{-3}$mm^2/s; D: $\times 10^{-3}$ mm^2/s; D*: $\times 10^{-3}$ mm^2/s; f*D*: $\times 10^{-3}$ mm^2/s. (Top and bottom of boxes: 25%-75% percentiles of data; line in box: median value; circles: outliers.)

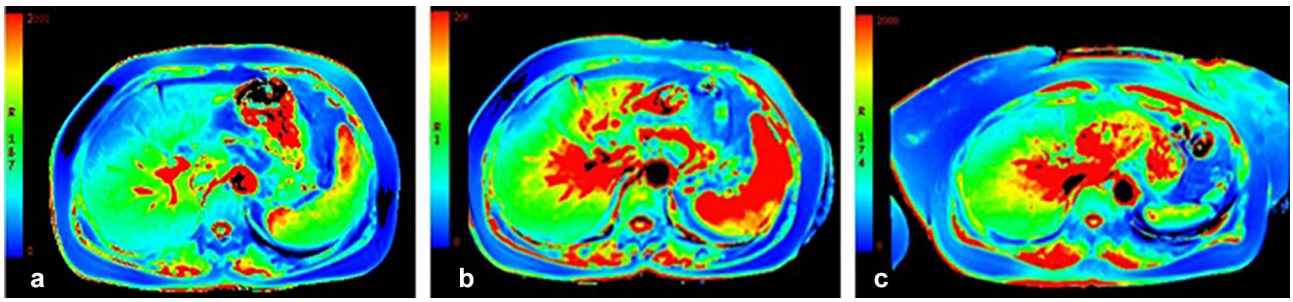

Fig. 4 T1 mapping of the liver. **a** A 55-year-old woman from 3-month follow-up group with decreased T1 relaxation time. **b** The same woman in (**a**) from 1-year follow-up group with slightly increased T1 relaxation time compared to figure (**a**). **c** A 55-year-old woman from control group with normal T1 relaxation time. (T1: msec)

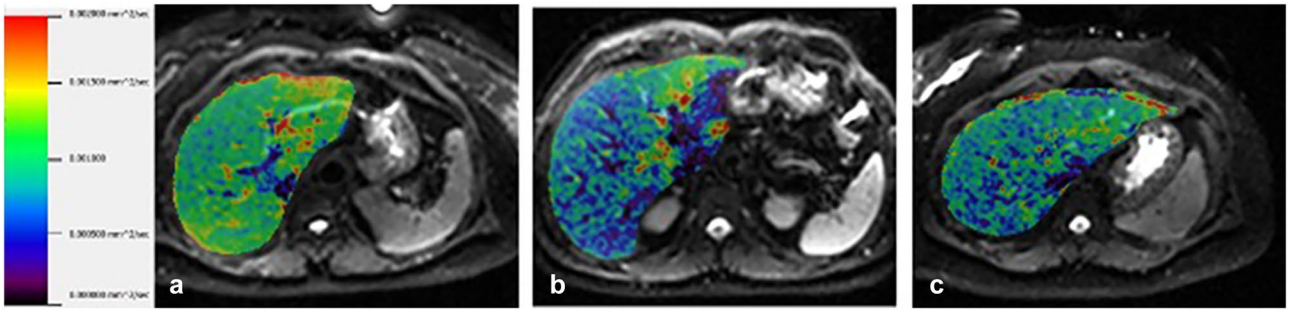

Fig. 5 IVIM-derived D value of the liver. **a** A 62-year-old woman from 3-month follow-up group with increased hepatic D value. **b** The same woman in (**a**) from 1-year follow-up group with decreased hepatic D value compared to figure (**a**). c A 34-year-old from control group with normal hepatic D value. (D: $\times 10^{-3}$ mm^2/s.)

and were significantly higher than the ones in the control group ($P=0.001$ and $P<0.001$, respectively). Medullary ADC values in both the 3-month and 1-year follow-up groups were significantly increased compared to the control group ($P=0.016$ and 0.002, respectively). The 1-year follow-up group had the highest medullary f*D* value, which was significantly higher than that in the control group ($P=0.032$). A detailed comparison between the two groups was shown in Fig. 7. The typical cases from the three groups were shown in Fig. 8. There were no differences of the parameters between the non-severe and

Table 4 Comparisons of T1 relaxation time and IVIM parameters of liver between non-severe and severe participants in the COVID-19 group

Parameters	Control ($n=24$)	Non-severe ($n=24$)	Severe ($n=13$)	P
T1	908.74 (888.22–964.83)	835.9 (766.3–893.0)	806.9 (745.4–892.3)	0.712
ADC	1.33 (1.11–1.68)	1.74 (1.37–2.09)	1.89 (1.77–2.31)	0.090
D	0.82 (0.75–0.95)	0.92 (0.83–1.01)	0.97 (0.85–1.08)	0.287
f	0.19 (0.13–0.27)	0.23 (0.18–0.29)	0.25 (0.21–0.28)	0.483
D*	40.27 (18.89–60.73)	37.3 (30.6–69.9)	62.9 (43.7–89.6)	0.031*
f*D*	6.08 (2.72–12.11)	9.8 (6.9–14.4)	13.9 (13.0–18.3)	0.015*

Data are expressed as median (P25-P75) for continuous variables

P values were comparisons between non-severe and severe participants calculated with Mann–Whitney U-test

*$P<0.05$ is considered to be statistically different

T1 T1 relaxation time(msec), *ADC* apparent diffusion coefficient ($\times 10^{-3}$ mm^2/s); *D* diffusion coefficient ($\times 10^{-3}$ mm^2/s)

D*: pseudo-diffusion coefficient ($\times 10^{-3}$ mm^2/s); f: perfusion fraction; f*D*: $\times 10^{-3}$ mm^2/s

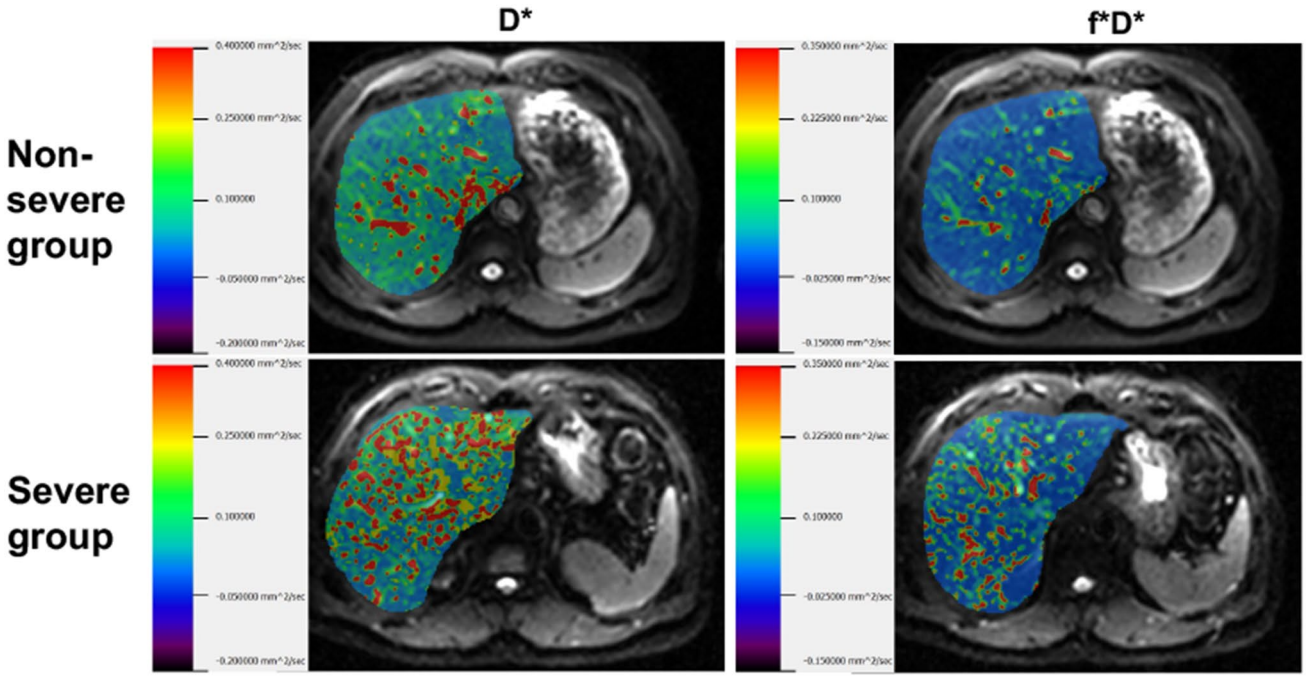

Fig. 6 Hepatic D* and f*D* values in a 47-year-old man with non-severe COVID-19 (top row) and a 54-year-old man with severe COVID-19 (bottom row). The severe case had higher hepatic D* and f*D* values than the non-severe case. (D*: $\times 10^{-3}$ mm^2/s; f*D*: $\times 10^{-3}$ mm^2/s.)

severe cases in the COVID-19 group (Table S2) and 1-year follow-up group (Table S4) (for all, $P>0.05$).

Discussion

In this study, lower hepatic T1 relaxation time and higher diffusion/perfusion parameters (including ADC, D, f, and f*D*) were found in the 3-month follow-up group of recovered COVID-19 patients compared with the control group of normal volunteers, with the hepatic D value decreasing significantly and the T1 relaxation time increasing slightly after a long-term follow-up. Recovered COVID-19 patients had higher renal ADC and f values at both short-term and long-term follow-ups. All these findings indicated that recovered COVID-19 patients might have developed liver and kidney impairments after infection, of which liver impairments were able to recover gradually and kidney impairments might exist for a long time.

According to our results, decreased T1 relaxation times and increased ADC, D, f, and f*D* values of the liver were detected in patients recovered from COVID-19 at 3-month

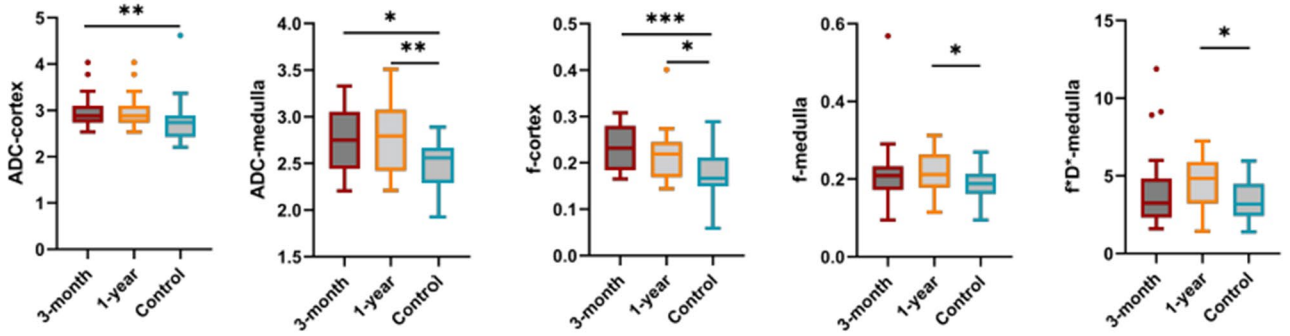

Fig. 7 Boxplots of IVIM-DWI parameters in the renal cortex and medulla of the three groups (*$P<0.05$; **$P<0.01$, ***$P<0.001$). Parameters without significant difference are not listed. *P* values between two independent groups were calculated using Mann–Whitney U-test. *P* values between paired variables (3-month follow-up group and 1-year follow-up group) were calculated using Wilcoxon Signed Rank Test. 3-month: 3-month follow-up group; 1-year: 1-year follow-up group; Control: control group. ADC: $\times 10^{-3}$ mm^2/s; D: $\times 10^{-3}$ mm^2/s; D*: $\times 10^{-3}$ mm^2/s; f*D*: $\times 10^{-3}$ mm^2/s. (Top and bottom of boxes: 25%-75% percentiles of data; line in box: median value; circles: outliers.)

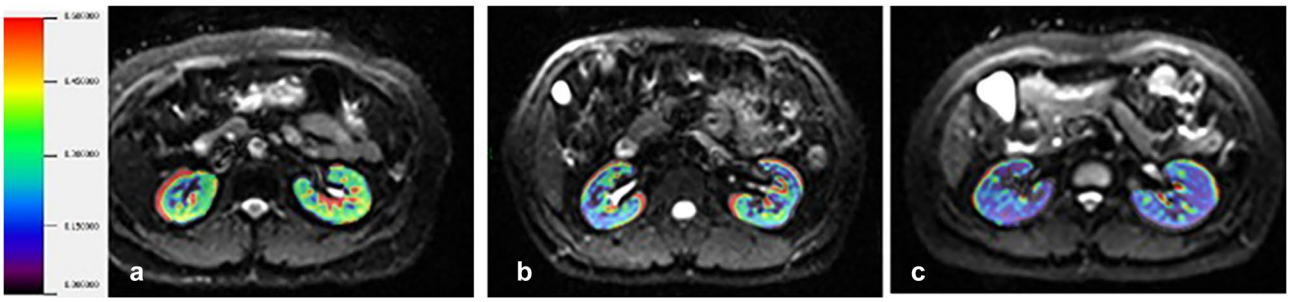

Fig. 8 IVIM-derived f value of the kidney. **a** A 59-year-old woman from 3-month follow-up group with increased renal f value. **b** The same woman in (**a**) from 1-year follow-up group with decreased renal f value compared to figure (**a**). C: A 36-year-old woman from control group with normal renal f value. (T1: msec; D: $\times 10^{-3}$ mm^2/s.)

follow-up. COVID-19 patients were proved to develop micro- or macro-vesicular steatosis pathologically, accompanied with inflammation, multifocal liver cell necrosis, sinusoidal dilatation, and congestion [18–20]. Thus, we assumed that the decreased T1 time might be attributed to hepatic steatosis. In addition, the liver is the major organ for synthesis of proteins involved in iron metabolism, including hepcidin and transferrin [21]. Hepatocyte impairment might result in iron deposition by reducing the production of hepcidin [21], which could shorten T1 consequently. Although the increased fluid caused by inflammation, necrosis, and congestion might lengthen T1, hepatic steatosis and iron deposition were expected to be the dominant micro-changes rather than acute tissue edema at the convalescence stage, which finally shortened T1 relaxation time. During the long-term follow-up, the T1 value showed mild elevation, probably indicating an incomplete recovery of hepatic steatosis and improved synthetic function via liver regeneration.

In this study, the inflammation-induced increased fluid in the interstitial space and focal hepatic necrosis in recovered COVID-19 patients were assumed to increase the D value [22]. Previous studies found that hepatic fat content might also lead to increased D and f values [23, 24], which is in line with our assumption. Except for steatosis, hepatic congestion accompanied by capillary dilatation and elevated permeability could also contribute to the elevated f and f*D* values. Compared to non-severe cases, severe cases had higher D* and f*D* values, demonstrating higher hepatic perfusion in severe COVID-19 cases. After long-term follow-up, the hepatic D value was significantly reduced, reflecting that the inflammation-induced interstitial edema and hepatic steatosis were relieved over time.

Increased ADC and f values from both the renal cortex and medulla were observed in recovered COVID-19 participants compared to normal volunteers. It was previously reported that in the kidneys, f value was not only related to vascular perfusion but also tubular fluid volume [12]. Based on the fact that SARS-CoV-2-infected patients could develop diverse tubular and glomerular diseases [25], we conjectured that the elevated f values could be due to the increased fluid loading caused by luminal dilatation reported in ATI [5, 26] In addition to the elevated perfusion, edematous expansion

of the interstitial space found in distal tubules and collecting ducts [26] might also account for increased ADC. No obvious reductions of cortical ADC and f values were noted at long-term follow-up, indicating the possible long-existing of tubular and glomerular damage in recovered COVID-19 patients.

Consistent with earlier studies [27], more free water diffusion in the renal cortex than the medulla resulted in higher cortical D values in all three groups. In this study, the tiny changes in D value at follow-ups indicated a smaller influence of SARS-CoV-2 infection on renal tissue diffusion than perfusion. Interestingly, the medullary f*D* value exhibited an increase at the long-term follow-up, suggestive of increased fluid loading during the recovery phase. However, the unstable D* value measured from the abdominal IVIM-DWI sequence could be another cause, and further study is needed to verify the speculation.

Liver and kidney MRI manifestations of COVID-19 patients have rarely been investigated in previous studies, especially the dynamic changes at follow-ups. To the best of our knowledge, this is the first prospective study using T1 mapping and IVIM-DWI to explore the functional imaging characteristics of the liver and kidneys in COVID-19 survivors. However, our study also has several limitations. First, T1 mapping with the VFA technique was sensitive to the inhomogeneity of the field and cardiac or respiratory motion artifacts, which could cause non-negligible bias. Second, the IVIM-MRI scans were performed using the free-breathing technique, which might affect the accuracy of the data. Third, laboratory tests were not obtained in normal volunteers to compare with COVID-19 participants. Finally, the sample size in this study was relatively small, especially the number of severe cases in the 1-year follow-up group. A future study that includes a larger population is needed to strengthen the statistical power.

Conclusion

In conclusion, the alterations of hepatic and renal imaging parameters detected with T1 mapping and IVIM-DWI were in line with the reported pathological findings in recovered COVID-19 patients. The dynamic changes of the imaging parameters indicated the potential reversibility of liver impairment and the long-existing kidney perfusion alterations.

Supplementary Information The online version contains supplementary material available at https://doi.org/10.1007/s00261-022-03471-y.

Author contributions Study design: QH, YL, YZ, XL, BY; Data collection: QH, YL, XL, AX, BY; Methodology: QH, YL, DW; Formal analysis: QH; Data interpretation: QH, YL, NM, YZ; Funding acquisition: BY, YL, XL, DW; Writing-original draft: QH; Writing-review & editing: QH, YL, BY. All authors contributed to the article and approved the submitted version.

Funding This project was supported by Clinical Research Plan of SHDC (Grant No. SHDC2020CR4069), Youth Program of National Natural Science Foundation of China (Fund No. 81901697), Shanghai Sailing Program (Grant No. 21YF1404800), Youth Program of Special Project for Clinical Research of Shanghai Municipal Health Commission Health industry (Grant No. 20204Y0421)and Youth Medical Talents—Medical Imaging Practitioner Program (No.3030256001).

Data availability The data and material that support the findings of this study are available from the corresponding author upon reasonable request.

Code availability The code that supports the findings of this study is available from the corresponding author upon reasonable request.

Declarations

Conflict of interest The authors declare that they have no known competing financial interests or personal relationships that are relevant to the content of this article.

Ethical approval Approval was obtained from the ethics committee of Huashan Hospital, Fudan University. Informed consent was obtained from all individual participants included in the study.

Consent to participate The ethics committee of our hospital approved our prospective study (No. 2021460), and waived the requirement of informed consent.

References

1. Chen N., M. Zhou, X. Dong, J. Qu, F. Gong et al (2020) Epidemiological and clinical characteristics of 99 cases of 2019 novel coronavirus pneumonia in Wuhan, China: a descriptive study. Lancet 395 (10223): 507-513. https://doi.org/10.1016/s0140-6736(20)30211-7
2. Zhang C., L. Shi, and F.S. Wang (2020) Liver injury in COVID-19: management and challenges. Lancet Gastroenterol Hepatol 5 (5): 428-430. https://doi.org/10.1016/s2468-1253(20)30057-1
3. Batlle D., M.J. Soler, M.A. Sparks, S. Hiremath, A.M. South et al (2020) Acute Kidney Injury in COVID-19: Emerging Evidence of a Distinct Pathophysiology. J Am Soc Nephrol 31 (7): 1380-1383. https://doi.org/10.1681/asn.2020040419
4. Gupta A., M.V. Madhavan, K. Sehgal, N. Nair, S. Mahajan et al (2020) Extrapulmonary manifestations of COVID-19. Nat Med 26 (7): 1017-1032. https://doi.org/10.1038/s41591-020-0968-3
5. Su H., M. Yang, C. Wan, L.X. Yi, F. Tang et al (2020) Renal histopathological analysis of 26 postmortem findings of patients with COVID-19 in China. Kidney Int 98 (1): 219-227. https://doi.org/10.1016/j.kint.2020.04.003
6. Hectors S.J., S. Riyahi, H. Dev, K. Krishnan, D.J.A. Margolis, and M.R. Prince (2021) Multivariate analysis of CT imaging, laboratory, and demographical features for prediction of acute kidney injury in COVID-19 patients: a Bi-centric analysis. Abdom Radiol (NY) 46 (4): 1651-1658. https://doi.org/10.1007/s00261-020-02823-w
7. Radenkovic D., S. Weingärtner, L. Ricketts, J.C. Moon, and G. Captur (2017) T(1) mapping in cardiac MRI. Heart Fail Rev 22 (4): 415-430. https://doi.org/10.1007/s10741-017-9627-2

8. Li Z., J. Sun, X. Hu, N. Huang, G. Han et al (2016) Assessment of liver fibrosis by variable flip angle T1 mapping at 3.0T. J Magn Reson Imaging 43 (3): 698-703. https://doi.org/10.1002/jmri.25030
9. Ding Y., S.X. Rao, T. Meng, C. Chen, R. Li, and M.S. Zeng (2014) Usefulness of T1 mapping on Gd-EOB-DTPA-enhanced MR imaging in assessment of non-alcoholic fatty liver disease. Eur Radiol 24 (4): 959-66. https://doi.org/10.1007/s00330-014-3096-y
10. Le Bihan D., E. Breton, D. Lallemand, P. Grenier, E. Cabanis, and M. Laval-Jeantet (1986) MR imaging of intravoxel incoherent motions: application to diffusion and perfusion in neurologic disorders. Radiology 161 (2): 401-7. https://doi.org/10.1148/radiology.161.2.3763909
11. Chen F., Y.L. Chen, T.W. Chen, R. Li, Y. Pu et al (2020) Liver lobe based intravoxel incoherent motion diffusion weighted imaging in hepatitis B related cirrhosis: Association with child-pugh class and esophageal and gastric fundic varices. Medicine (Baltimore) 99 (2): e18671. https://doi.org/10.1097/md.0000000000018671
12. Sigmund E.E., P.H. Vivier, D. Sui, N.A. Lamparello, K. Tantillo et al (2012) Intravoxel incoherent motion and diffusion-tensor imaging in renal tissue under hydration and furosemide flow challenges. Radiology 263 (3): 758-69. https://doi.org/10.1148/radiol.12111327
13. Ichikawa S., U. Motosugi, T. Ichikawa, K. Sano, H. Morisaka, and T. Araki (2013) Intravoxel incoherent motion imaging of the kidney: alterations in diffusion and perfusion in patients with renal dysfunction. Magn Reson Imaging 31 (3): 414-7. https://doi.org/10.1016/j.mri.2012.08.004
14. Uchida Y., H. Uemura, S. Yamaba, D. Hamada, N. Tarumoto et al (2020) Significance of liver dysfunction associated with decreased hepatic CT attenuation values in Japanese patients with severe COVID-19. J Gastroenterol 55 (11): 1098-1106. https://doi.org/10.1007/s00535-020-01717-4
15. Idilman I.S., G. Telli Dizman, S. Ardali Duzgun, I. Irmak, M. Karcaaltincaba et al (2021) Lung and kidney perfusion deficits diagnosed by dual-energy computed tomography in patients with COVID-19-related systemic microangiopathy. Eur Radiol 31 (2): 1090-1099. https://doi.org/10.1007/s00330-020-07155-3
16. The Guidelines for the Diagnosis and Treatment of New Coronavirus Pneumonia, 7th edition, National Health Commission of the People's Republic of China. China, 2020.
17. Cassinotto C., M. Feldis, J. Vergniol, A. Mouries, H. Cochet et al (2015) MR relaxometry in chronic liver diseases: Comparison of T1 mapping, T2 mapping, and diffusion-weighted imaging for assessing cirrhosis diagnosis and severity. Eur J Radiol 84 (8): 1459-1465. https://doi.org/10.1016/j.ejrad.2015.05.019
18. Wang Y., S. Liu, H. Liu, W. Li, F. Lin et al (2020) SARS-CoV-2 infection of the liver directly contributes to hepatic impairment in patients with COVID-19. J Hepatol 73 (4): 807-816. https://doi.org/10.1016/j.jhep.2020.05.002
19. Ji D., E. Qin, J. Xu, D. Zhang, G. Cheng et al (2020) Non-alcoholic fatty liver diseases in patients with COVID-19: A retrospective study. J Hepatol 73 (2): 451-453. https://doi.org/10.1016/j.jhep.2020.03.044
20. Sonzogni A., G. Previtali, M. Seghezzi, M. Grazia Alessio, A. Gianatti et al (2020) Liver histopathology in severe COVID 19 respiratory failure is suggestive of vascular alterations. Liver Int 40 (9): 2110-2116. https://doi.org/10.1111/liv.14601
21. Milic S., I. Mikolasevic, L. Orlic, E. Devcic, N. Starcevic-Cizmarevic et al (2016) The Role of Iron and Iron Overload in Chronic Liver Disease. Med Sci Monit 22 2144-51. https://doi.org/10.12659/msm.896494
22. Yu S.M., S.H. Ki, and H.M. Baek (2015) Nonalcoholic Fatty Liver Disease: Correlation of the Liver Parenchyma Fatty Acid with Intravoxel Incoherent Motion MR Imaging-An Experimental Study in a Rat Model. PLoS One 10 (10): e0139874. https://doi.org/10.1371/journal.pone.0139874
23. Guiu B., J.M. Petit, V. Capitan, S. Aho, D. Masson et al (2012) Intravoxel incoherent motion diffusion-weighted imaging in non-alcoholic fatty liver disease: a 3.0-T MR study. Radiology 265 (1): 96-103. https://doi.org/10.1148/radiol.12112478
24. Joo I., J.M. Lee, J.H. Yoon, J.J. Jang, J.K. Han, and B.I. Choi (2014) Nonalcoholic fatty liver disease: intravoxel incoherent motion diffusion-weighted MR imaging-an experimental study in a rabbit model. Radiology 270 (1): 131-40. https://doi.org/10.1148/radiol.13122506
25. Ahmadian E., S.M. Hosseiniyan Khatibi, S. Razi Soofiyani, S. Abediazar, M.M. Shoja et al (2021) Covid-19 and kidney injury: Pathophysiology and molecular mechanisms. Rev Med Virol 31 (3): e2176. https://doi.org/10.1002/rmv.2176
26. Ahmadian E., S.M. Hosseiniyan Khatibi, S. Razi Soofiyani, S. Abediazar, M.M. Shoja et al (2020) Covid-19 and kidney injury: Pathophysiology and molecular mechanisms. Rev Med Virol e2176. https://doi.org/10.1002/rmv.2176
27. Liang L., W.B. Chen, K.W. Chan, Y.G. Li, B. Zhang et al (2016) Using intravoxel incoherent motion MR imaging to study the renal pathophysiological process of contrast-induced acute kidney injury in rats: Comparison with conventional DWI and arterial spin labelling. Eur Radiol 26 (6): 1597-605. https://doi.org/10.1007/s00330-015-3990-y